Response to Referee 1

From the center of wind pressure to loads on the wind turbine: A stochastic approach for the reconstruction of load signals

Referee's comment (RC) in blue
Author's comment (AC) in black

The references to lines in the manuscript (e.g., 'L.80') are given with respect to the **new version** of the paper.
In gray: text from the revised version of the manuscript.

GENERAL COMMENTS

REFEREE:

The method proposed by the authors is intended to enable a fast estimation of the Damage Equivalent Load (DEL) over very long time histories (years). The comparison between DEL, DEL_{CoWP}, and DEL_{CoWP_R} is satisfactory, but not excellent: the slope of the interpolation line is clearly below one, and there is a notable spread of data around the fitted line. The authors do not comment on how this discrepancy might affect the DEL estimation over long time periods. Should we expect differences in the order of 1%, 5%, 10%, 30%, or even 50%?

Thank you for your comment. We recognize that the current capacity of the method was not accurately stated in the manuscript. At its current state, our method is not sufficient for calculating the DELs over long-time periods. Instead, we present simple concepts with which the calculation of the long-period DELs will be easily possible.

Further considerations should be considered with the method proposed in the paper, for the complete calculation of the DELs over the lifetime of a WT. First, a transfer function for calibrating the normalized magnitudes of the CoWP to the magnitudes of the bending moments should be derived, for example, from corresponding data of a wind turbine of interest. Second, a model for the high-frequency component of the loads needs to be implemented. Third, the long-term wind conditions (e.g., Weibull distribution) at a specific location must be known.

A few lines have been incorporated and/or modified in the manuscript to correctly describe the current capability of the method, as well as to state the future steps to be included for a complete assessment of the loads in the context of long-time calculations.

L.82: In its current state, the method is limited to the modeling of the dynamics of the low-frequency components of the bending moments. However, when com-

bined with a description of the high-frequency components, a validated rescaling procedure, and the characterization of the site-specific wind conditions, this approach enables a novel method for a fast assessment of the lifetime loads in WTs.

L.166: However, the implementation of the stochastic method for lifetime load assessment in engineering applications (i.e., including both the high- and low-frequency components of the loads) is constrained in its application. To ensure a comprehensive lifetime model, it is necessary to incorporate additional elements. A turbine-specific transfer function for rescaling the magnitudes of the loads is required. A complementary model for the high-frequency components of the loads must be integrated. Finally, the occurrence of the loads must be weighted by the distribution of the mean wind speed at the location of the WT (e.g., annual Weibull distribution).

The method can predict DELs associated with the low-frequency component of the loads. However, the overall DEL also includes high-frequency loads, which are characterized by many cycles. The authors do not comment on the difference between DELs from low-frequency load components and total DELs.

Thank you for the comment. In fact, the difference between the DELs from low-frequency load components and DELs from total loads has not been discussed in the paper. In the following, an analysis of the contribution to the DELs of low-frequency and high-frequency components of the loads is shown.

Three signals are compared. The low-frequency signal ('Low freq.') corresponds to the low-pass filtered load described in Sec. 4 in the manuscript with a cutoff frequency of $f_{cutoff} = 0.1$Hz. The high-frequency signal ('High freq.') corresponds to the load fluctuations with frequency over f_{cutoff}. The total load ('Total') is the estimated load from BEM simulations, which aggregates both the high- and the low-frequency contributions. The investigated load signals are those calculated for the 5MW NREL WT with Kaimal fields, with $\bar{u} = 7$m/s (see Sec. 3 in the manuscript).

Figure A shows an excerpt of the time series of the three signals (Total, Low freq., and High freq.) over 1200s for the T_{titlt} at the main shaft of the WT.

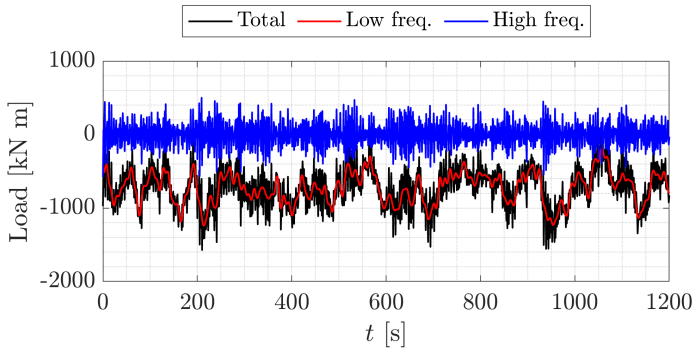

Figure A: 20-min excerpt of the load signals (Total, Low freq., and High freq.), for the T_{titlt} at the main shaft.

Now, the DELs of the three signals are investigated. Fig. B(a) shows the DELs calculated over periods T = 60s along the same 1200s shown in Fig. A. A fourth signal, 'Sum L+H' is included. It corresponds to the combination of the DELs (i.e., not the time series) from the low- and high-frequency signals as,

$$(\mathrm{DEL}_{\mathrm{Sum\ L+H}}) = \alpha\,(\mathrm{DEL}_{\mathrm{Low}}) \;+\; \beta\,(\mathrm{DEL}_{\mathrm{High}}), \tag{1}$$

calculated for each period T. The parameters α and β are fitting parameters to achieve $\mathrm{DEL}_{\mathrm{Sum\ L+H}} \approx \mathrm{DEL}_{\mathrm{Total}}$. These parameters depends on the Wöhler coefficient m and the length T for the calculation of $\mathrm{DEL}_{\mathrm{Low}}$ and $\mathrm{DEL}_{\mathrm{High}}$. In Fig. B(a), the parameters are $\alpha = 1.2$, and $\beta = 0.5$. The values of the coefficients α and β from the load signals can be taken as weighting factors, indicating a dominating contribution of the $\mathrm{DEL}_{\mathrm{Low}}$ with respect to $\mathrm{DEL}_{\mathrm{High}}$. For the case shown, the proportion is approximately $2:1$.

Fig. B(b) shows the correlation between the DELs of the original 'Total', and the added 'Sum L+H'. The correlation is calculated for the DELs along the entire data set ($4.7\mathrm{x}10^4$ s).

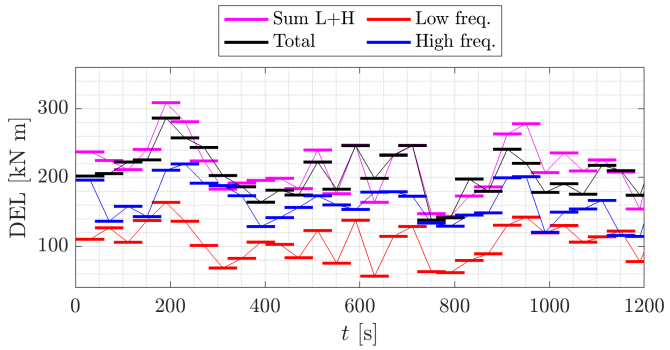

(a)

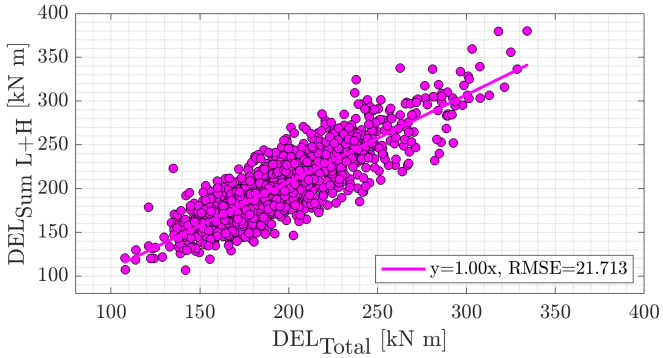

(b)

Figure B: (a) 20-min excerpt of the DELs for the T_{titlt} signals at the main shaft. The length of the individual horizontal bars depicts the periods T. (b) Correlation plot between the total load and the sum of the DELs from the low- and high-frequency signals. The DELs are calculated with $m = 10$ over periods of T = 60s with an overlap of 30s between periods.

In our paper, we concentrated entirely on the low-frequency events. This choice is based on the particular interest of our research partners. However, for a complete calculation of the DELs on the WT, a second model for the high-frequency component is required. The use of Gaussian distributed noise is proposed as a first approach. Three random Gaussian realizations, 'R1', 'R2', and 'R3', with the statistics from the original high-frequency load signal, are generated. The considered statistics include not only the mean and standard deviation, but also the correlation and dominant frequency. Fig. C(a) shows an excerpt of the time series of the original and the random Gaussian signals. In (b), the corresponding PDFs are shown. A Gaussian distribution fitted to the PDF of the original 'High freq.' is depicted by the solid black line.

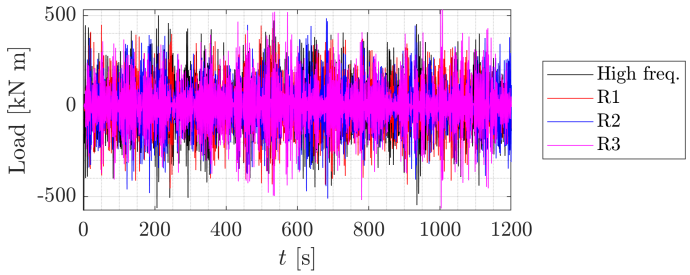

(a)

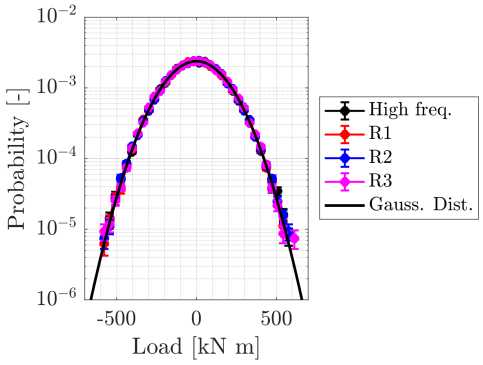

(b)

Figure C: High-frequency signals of the original load signal ('High-freq') and three realizations of Gaussian-distributed noise ('R1', 'R2', and 'R3'). (a) 20-min excerpt of the time series. (b) PDFs of the signals. The solid line in (b) depicts a Gaussian distribution.

Next, the four high-frequency signals are added to the low-frequency component of the load. Then, the DELs are calculated. Fig. D(a) shows a 20-min excerpt of the DELs. Fig. D(b) shows a box-plot of the DELs over the entire time series ($4.7\text{x}10^4$ s).

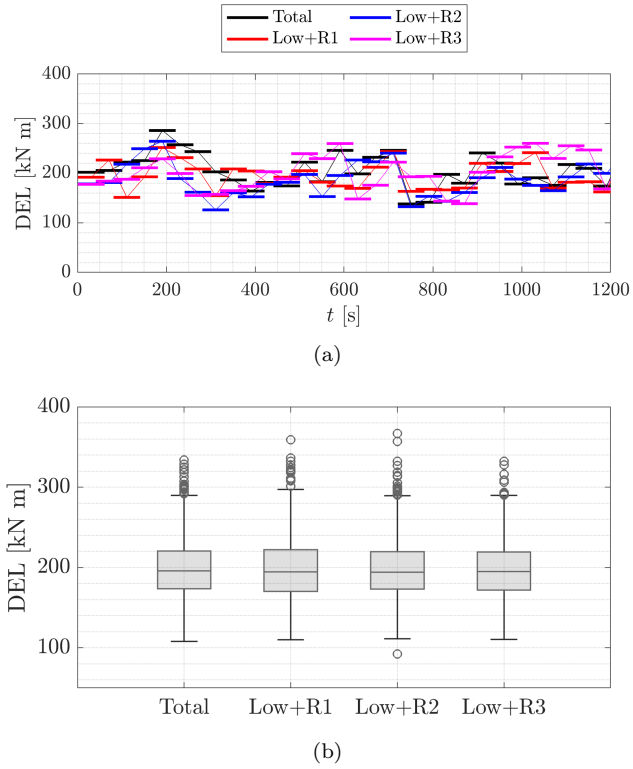

Figure D: DELs of the total signals (low-frequency and high-frequency signals). (a) 20-min excerpt with individual DELs. (b) Box-plots of the DELs along the entire time series. The four high-frequency signals ('High freq.', 'R1', 'R2', and 'R3') have been added to the same low-frequency signal. The DELs are calculated with $m = 10$ over periods of T = 60s with an overlap of 30s between periods.

The comparability of the PDFs in Fig. C and the boxplots in Fig. D shows that Gaussian noise, with parametrized dominant frequency and correlation, can be used as a model for the high-frequency component of the load signals. Then, this Gaussian model for high-frequency fluctuations might be used in combination with our proposed model, based on the CoWP, which reproduced the low-frequency component of the load signal. Then, an entire model of the load could be achieved. The joint use of these two models must be further validated by comparing them to the total simulated loads. For that, a transfer function is required for scaling the magnitudes of the loads.

Given the relevance of commenting about the DEL calculated from the low-frequency component and the total load signals, **Appendix B** has been incorporated into the manuscript, which partially includes the analysis previously

shown. Additionally, the lines below have been modified.

L.293-299: It is essential to acknowledge that the discussion on the DELs presented in our work is exclusively focused on the DELs from the low-frequency component of the signals. This choice is based on a particular interest of our research partners. In order to assess the complete DELs (e.g., from both the low- and high-frequency load events), it is necessary to establish an additional model for incorporating the contribution from the high-frequency signal. In this direction, a simple surrogate stochastic model has shown satisfactory results. The characteristics of the original high-frequency load signal are well reproduced. The proposed stochastic model for the high-frequency signals, and calculations on the differences between the DELs from the low- and high-frequency load components, and total DELs are shown in Appendix B.

The simulations using Kaimal data are performed at a single mean wind speed, under partial load conditions (region II). What is the impact of turbine control on the accuracy of the proposed method? It would be useful to compare the results with wind speeds above the rated.

Thank you for the comment. You are right, in the paper, only a single mean wind speed, included within the region II, is presented. In the following, we show the results of the analysis for the case with $\bar{u} = 13\text{m/s}$ (i.e., above the rated), by using standard Kaimal wind fields.

Figure E shows the time series of $\bar{u}$ at hub height. Fig. F is equivalent to Fig. 5 in the manuscript. It shows the comparison between the time series of the normalized signals of the CoWP and the bending moments at the main shaft.

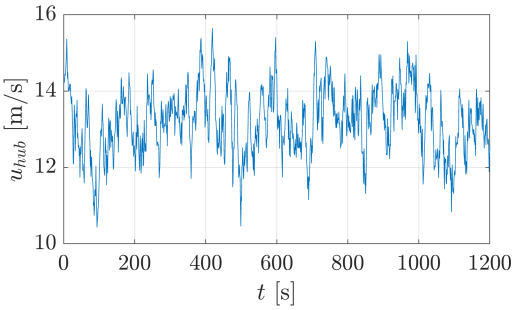

Figure E: 20-min excerpt of the wind speed $u(t)$ at hub height.

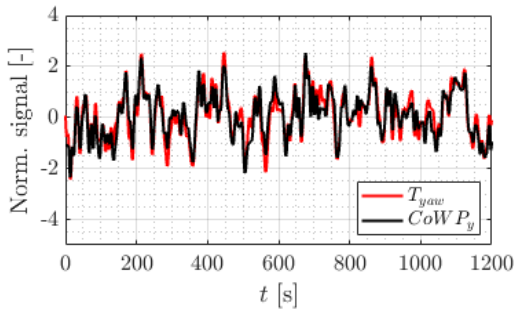

(a)

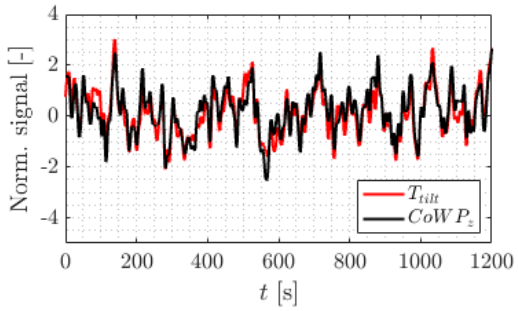

(b)

Figure F: 20-min excerpts of the CoWP and the bending moments at the main shaft of a WT. (a) T_{yaw} and CoWP_y, and (b) T_{tilt} and CoWP_z. The signals are normalized and low-pass filtered.

Figure G is equivalent to Fig. 6 in the manuscript. The correlation between the signals is shown.

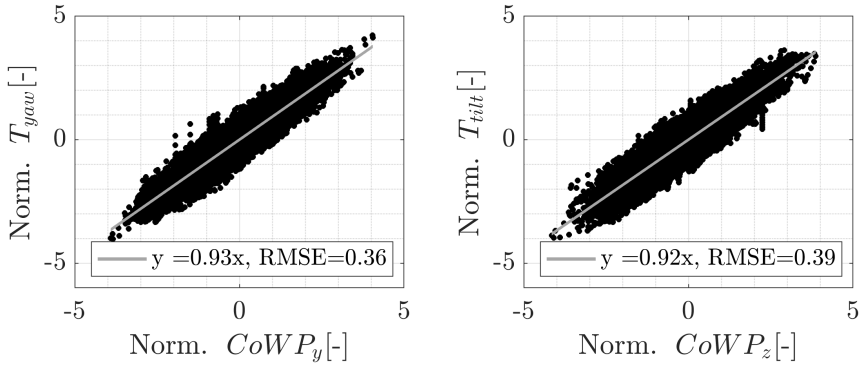

(a) (b)

Figure G: CoWP against the bending moments plotted as $(CoWP(t), T(t))$ for each time step t of the time series. In (a) T_{yaw} and CoWP_y, and (b) T_{tilt} and CoWP_z. The gray lines depict linear fittings $T = a\ (CoWP)\ +\ b$. The signals are normalized and low-pass filtered.

Lastly, Fig. H is equivalent to Fig. 8 in the manuscript. The correlation plots between the DEL and DEL_{CoWP} are shown in (a) and (b). The corresponding box plots are presented in (c) and (d).

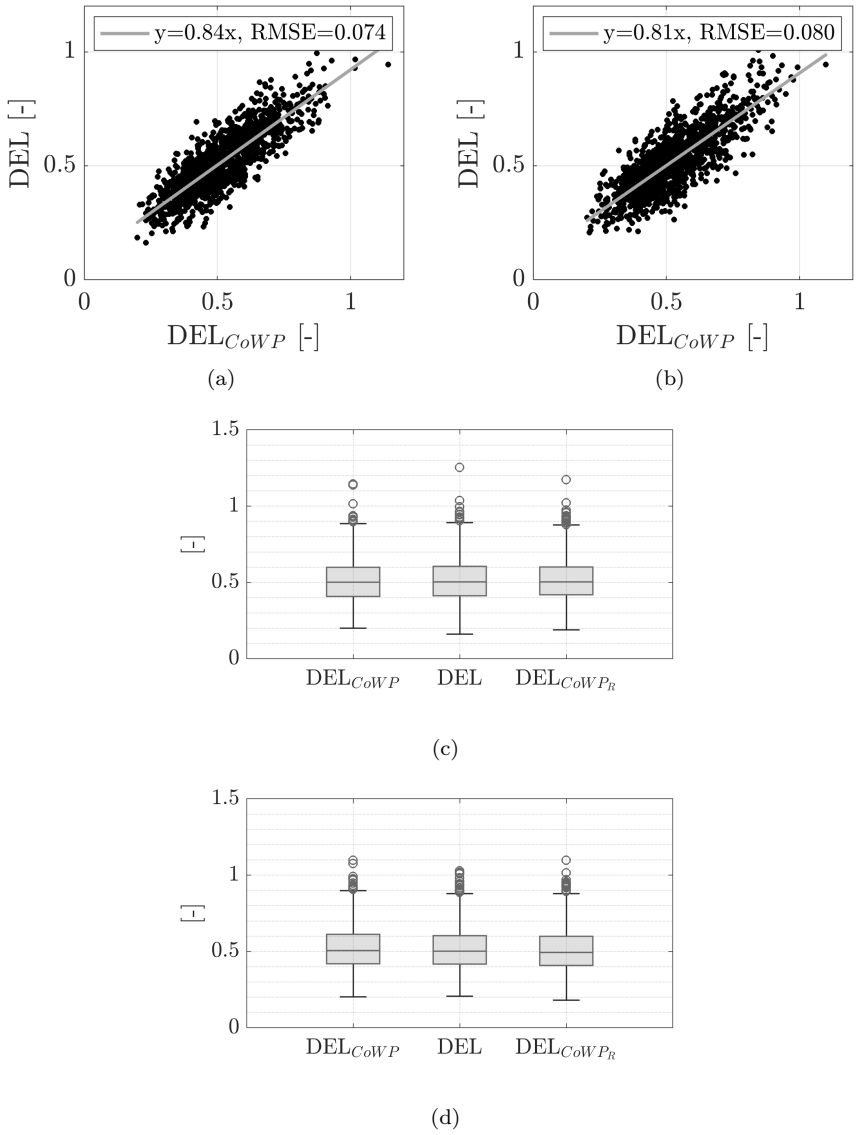

Figure H: Comparison between the DEL and $\mathrm{DEL_{CoWP}}$. Correlation plots and box plots for CoWP_y and T_{yaw} in (a) and (c), and CoWP_z and T_{tilt} in (b) and (d). The gray lines in (a) and (b) depict linear fittings. In the box plots in (c) and (d), the horizontal line inside each box shows the median, and the bottom and top edges indicate the 25th and 75th percentiles. The whiskers indicate the most extreme data points. The markers show outliers. The DEL and $\mathrm{DEL_{CoWP}}$ are calculated with $m = 10$ over periods T = 60 s with 30 s overlapping between two consecutive periods. The signals are normalized and low-pass filtered.

Both, the correlation between the time series of the CoWP and the bending moments (Figs. F and G), and their corresponding DEL and $\mathrm{DEL}_{\mathrm{CoWP}}$ in Fig. H, show that the results for $\bar{u} = 13\mathrm{m/s}$ are comparable to those presented in the paper for $\bar{u} = 7\mathrm{m/s}$. Accordingly, the proposed method for estimating large-scale dynamics of the bending moments based on the CoWP from the wind holds for wind speeds above rated.

Accordingly, L.291 has been added to the manuscript.

The validity of the method has been proven for the rated power regime of the WT.

There is no discussion on how the proposed method could be integrated into current engineering practice, which involves estimating total DELs (including both low- and high-frequency components) from 10-minute simulations. In other words, how can the DELs associated with low-frequency atmospheric variations (predictable using the CoWP or its surrogate) be integrated with those due to high-frequency atmospheric fluctuations?

Thank you very much for your comment. The authors agreed on the high relevance of the question. Consequently, we included a paragraph in the conclusions of the manuscript L.393-412 for discussing how the proposed method can be incorporated into engineering applications.

However, the development of lifetime predictions in engineering applications necessitates the incorporation of additional elements in conjunction with the proposed stochastic method for modeling the low-frequency component of the loads. Initially, a turbine-specific transfer function for rescaling the CoWP to the magnitudes of the low-frequency component of the bending moments should be derived. Secondly, a numerical model of the high-frequency component of the loads is required. A stochastic Gaussian model has been demonstrated to be a viable approach. Thirdly, site-specific wind characteristics should be considered. These characteristics should include the long-term standard wind conditions, such as the annual Weibull distribution of the wind speed. Additionally, spatial descriptions (i.e., perpendicular to the main flow) of the wind structures are necessary to describe the dynamics of the CoWP at the given location. These spatial descriptions may be derived either from measured data over a two-dimensional area (e.g., using LiDAR techniques), or from accurately modeled wind data, which includes realistic information about the wind structures in the spatial domain. Once the three complementary elements have been resolved, the complete prediction of the yaw and tilt bending moments at the main shaft of a turbine can be applied as follows: site-specific wind data over relatively short intervals (e.g., 10 minutes), which are used for the calculation of the CoWP. Subsequently, the dynamics of the large-scale wind structures described by the CoWP are derived by using the Langevin stochastic approach. The parameters of the Langevin model for the specific wind conditions (i.e., drift and diffusion coefficients) are then estimated. Next, stochastic realizations

of the low-frequency component of the loads are generated by combining the dynamics of the CoWP and the previously determined turbine-specific transfer function. Afterwards, the high-frequency component is modeled. Subsequently, the high- and low-frequency load signals, which have been modeled independently, are combined. Finally, the long-term distribution of the mean wind speed $p(\bar{u})$ at the specific location is used to assess the entire lifetime damage of the bending moments (i.e., by applying the standard IEC procedure for load assessment based on mean wind speed binning and design load cases).

The analysis focuses on DELs. However, wind turbines are also designed to withstand ultimate loads. Could the proposed approach be useful in this context as well? Is there any correlation between CoWP and ultimate hub loads?

Thank you very much for the question. As you have appropriately mentioned, the assessment of ultimate loads is as essential as the corresponding fatigue predictions (e.g., DELs). In principle, the CoWP might be directly correlated to ultimate loads on the WT. When coherent structures, such as localized gusts, are responsible for the ultimate loads on the WT, our CoWP approach could correctly predict the maximum loads.

However, the correlation between extreme loads and localized structures remains an open question for the wind industry. The gusts defined by the IEC under extreme conditions are assumed to be homogeneous (i.e., over the entire rotor plane). For modern large wind turbines, however, it is expected that gusts are spatially inhomogeneous and affect the rotor as localized structures. Further analysis of atmospheric wind fields is needed. Long-term wind field measurements are required. Accurate modeling of localized, coherent wind structures would enable our approach to be applied to ultimate load calculations.

The section on data availability is missing. If possible, the authors should share both the data and the scripts used.

Thank you for the suggestion. We are working on providing the scripts and an exemplary data set. Together, they could be used for calculating the CoWP and applying the stochastic method for reconstructing random signals of the loads.

SPECIFIC COMMENTS

Section 2.2 (Damage Equivalent Load): This section summarizes well-known information about DEL calculation, already available in IEC guidelines. It should be omitted.

We appreciate your recommendation. However, we consider that describing the DEL along Section 2.2 and in Eq.(5) in the manuscript is essential for the afterward introduction of the $\mathrm{DEL}_{\mathrm{CoWP}}$ in Eq.(12).

Nevertheless, the section has been shortened by removing some details that, as you mentioned, are not highly relevant for the manuscript and are already available in the IEC standard.

Figure 8: What exactly do the whiskers represent? The caption mentions they indicate the most extreme data points, but does not specify how these are defined (e.g., 95% or 99% confidence interval?).

The whiskers in the boxplots (Figs. 8a, 8b, 13a, 13b, 19a and 19b) represent the outlier threshold based on the interquartile range (IQR) method. In this case, the $1.5 \times$ IQR rule is applied. Then, the length of the whiskers are calculated as $Q1 - (1.5 \times \text{IQR})$ and $Q3 + (1.5 \times \text{IQR})$, with $\text{IQR} = Q3 - Q1$.

A more complete definition of the whiskers is provided in the caption of the figures. Note that instead of quartiles, percentiles are used in the paper.

Lines [prev.]221–222: The cut-off frequency used for filtering CoWP and loads should be close to the 3P frequency. However, the authors use 0.1 Hz, which is significantly lower than the 3P frequency of the NREL 5MW turbine operating at rated power (approximately 0.6 Hz). The reason for this choice is unclear. The type and order of the filter should also be specified.

Thank you for noticing this inconsistency.

The mean wind speed at the hub is set to $\bar{u} = 7$m/s (see Sect. 3). Then, the NREL 5MW is operating at around 9rpm, or P ≈ 0.15Hz. Correspondingly, 3P≈ 0.45Hz. However, it is not true that the applied filter is of the order of the 3P frequency, as we mistakenly stated in L.221.

Certainly, the cutoff frequency of the filter should be lower than the 3P and P frequencies to remove the effect of the gravitational loads. Therefore, the selection of f_{cutoff} is rather constrained by the P frequency.

Fig. I shows the spectrum $E(f)$ of the CoWP in the horizontal direction and the yaw bending moment. As observed, the agreement on the frequency content between the signals remains up to $f = 0.1$Hz. At higher frequencies, the load signal deviates to larger fluctuations. Accordingly, only wind and load events with $f > 0.1$Hz (i.e., with temporal scales larger than 10s are investigated).

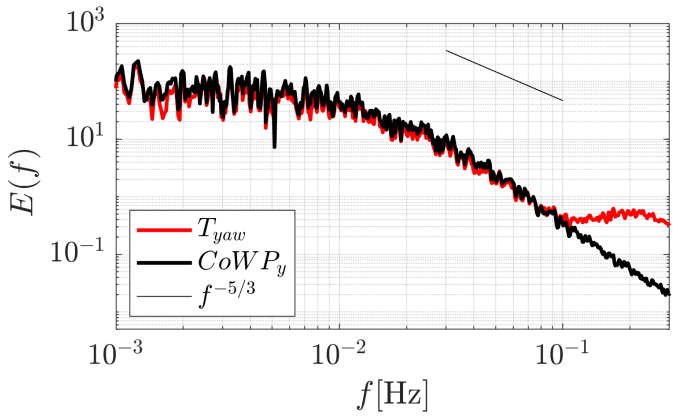

Figure I: Energy spectrum of the CoWP in the horizontal direction and the yaw bending moment.

The filter is a finite impulse response (FIR) filter with the pass-band frequency f_{cutoff}.

L.251 has been modified in the manuscript.

The filter is a finite impulse response (FIR) filter with the cutoff or pass-band frequency f_{cutoff}. The value of f_{cutoff} should be lower than the rotational frequency P of the WT.

Figure 8: Why is the correlation between DEL and DEL$_{CoWP}$ better for the T_{yaw} loads (left-right CoWP displacement) than for T_{tilt} loads (up-down CoWP displacement)?

Thank you for the question. A better agreement between the DEL and DEL$_{\mathrm{CoWP}}$ for the T_{yaw} compared to the T_{tilt} in Fig.8 can be explained by the correlation between the time series of the CoWP and the bending moments shown in Fig. 6 in the manuscript.

In Fig. 6, the slopes indicate a very good correlation for both, T_{yaw} in (a), and T_{tilt} in (b), with respect to the CoWP. However, the results of the T_{tilt} in (b) are slightly more scattered compared to T_{yaw}. The scattering is quantified by a higher value of the Root Mean Squared Error (RMSE). Such stronger or more frequent differences between the T_{tilt} and the $CoWP_z$ explain the lower correlation of the corresponding DELs in Fig. 8(b).

We consider that your question is worth addressing in the manuscript. L. 285 has been added.

[In Fig.8] A lower correlation is obtained for the DEL and DEL$_{\mathrm{CoWP}}$ in the vertical direction in panel (b) compared to the horizontal component shown in (a). The lower correlation is explained by the more scattered results within

the correlation of the time series of the T_{tilt} and the $CoWP_z$ shown in Fig.6. There, a value of RSME = 0.40 indicates a higher degree of scattering for T_{tilt}, compared to a RSME = 0.34 for T_{yaw}.

Figures 10, 16, [prev.]D2: The CoWP is defined with respect to the center of the rotor disk. Therefore, the $CoWP_z$ should oscillate around 90 m (Kaimal data) or 125 m (GROWIAN data). This is not evident in the figures.

You are entirely right. The $CoWP_z$ should oscillate around 90 m for the Kaimal fields, and 125 m for the GROWIAN data. Accordingly, the trajectories of the CoWP are shown in Figs. 10, 16, and E2 exhibit the vertical component $CoWP_z$ (y-axis) around 90m or 125m, respectively. Notably, the trajectories in Fig. E2 are shifted upwards ($CoWP_z$ around 95 m) due to the wind shear.

Figures 8a, 8b, 19a, 19b: It would be helpful to include the RMSE values.

Thank you for the comment and suggestion.

The RMSE values have been included in all the figures illustrating a linear fitting (i.e., Figures 6a, 6b, 8a, 8b, 14a, 14b 19a, and 19b).

A new version of the manuscript is provided along with a diff file.

References

[1] Schubert, C., Moreno, D., Schwarte, J., Friedrich, J., Wächter, M., Pokriefke, G., Radons, G., and Peinke, J.: Introduction of the Virtual Center of Wind Pressure for correlating large-scale turbulent structures and wind turbine loads, Wind Energy Sci. Discuss. [preprint], 2025, 1–19, https://doi.org/10.5194/wes-2025-28, *in review*, 2025.